Anisotropic plasmonic Cu nanoparticles in sol-gel oxide nanopillars studied by spectroscopic Mueller matrix ellipsometry

Z. Ghadyani,[1] M. Kildemo,[1,*] L. M. S. Aas,[1] Y. Cohin,[2] and E. Søndergård[2]

[1]*Department of Physics, Norwegian University of Science and Technology (NTNU), NO-7491, Norway*

[2]*Surface du Verre et Interfaces, Unit Mixte de Recherche CNRS/Saint-Gobain, UMR 125, 39 Quai Lucien Lefranc, F-93303 Aubervilliers Cedex, France*

[*]*morten.kildemo@ntnu.no*

Abstract: Broadened plasmon resonances of Cu nanoparticles in nanopatterned mixed oxide sol-gel nanopillars are shown to be readily detected by spectroscopic Mueller matrix ellipsometry. The plasmonic nanomaterials are obtained by low energy ion sputtering of a CuO sol-gel film. Both s- and p-polarized plasmon resonances are observed in the off-block-diagonal and the block-diagonal Mueller matrix elements as well as in the generalized ellipsometric parameters. The resonant features in all elements correlate with both maximum depolarization and a minimum in the reflected intensity. The spectral position and the polarization character of the plasmon resonances are discussed phenomenologically through effective medium theory.

OCIS codes: (300.0300) Spectroscopy; (120.2130) Ellipsometry and polarimetry; (250.5403) Plasmonics; (040.5350) Photovoltaic; (160.4236) Nanomaterials.

References and links

1. H. G. Tompkins and E. A. Irene, *Handbook of Ellipsometry* (William Andrew Inc., 2005).
2. H. Fujiwara, ed., *Spectroscopic Ellipsometry: Principles and Applications* (John Wiley & Sons Ltd., 2007).
3. N. Guth, B. Gallas, J. Rivory, J. Grand, A. Ourir, G. Guida, R. Abdeddaim, C. Jouvaud, and J. de Rosny, "Optical properties of metamaterials: Influence of electric multipoles, magnetoelectric coupling, and spatial dispersion," Phys. Rev. B **85**, 115138 (2012).
4. D. Schmidt, B. Booso, T. Hofmann, E. Schubert, A. Sarangan, and M. Schubert, "Monoclinic optical constants, birefringence, and dichroism of slanted titanium nanocolumns determined by generalized ellipsometry," Appl. Phys. Lett. **94**, 011914 (2009).
5. I. S. Nerbø, S. Le Roy, M. Foldyna, E. Søndergård, and M. Kildemo, "Real-time in situ Mueller matrix ellipsometry of GaSb nanopillars: observation of anisotropic local alignment." Opt. Express **19**, 12551–12561 (2011).
6. T. Oates and A. Mücklich, "Evolution of plasmon resonances during plasma deposition of silver nanoparticles," Nanotechnology **16**, 2606 (2005).
7. I. Nerbø, S. L. Roy, M. Kildemo, and E. Søndergård, "Real-time in situ spectroscopic ellipsometry of GaSb nanostructures during sputtering," Appl. Phys. Lett. **94**, 213105 (2009).
8. I. S. Nerbø, S. Le Roy, M. Foldyna, M. Kildemo, and E. Søndergård, "Characterization of inclined GaSb nanopillars by Mueller matrix ellipsometry," J. Appl. Phys. **108**, 014307 (2010).
9. L. Aas, M. Kildemo, Y. Cohin, and E. Søndergård, "Determination of small tilt angles of short gasb nanopillars using uv-visible mueller matrix ellipsometry," Thin Solid Films **541**, 97–101 (2012).
10. P. Wang, X. Zhao, and B. Li, "ZnO-coated CuO nanowire arrays: fabrications, optoelectronic properties, and photovoltaic applications," Opt. Express **19**, 11271 (2011).

#197582 - $15.00 USD Received 12 Sep 2013; revised 18 Nov 2013; accepted 27 Nov 2013; published 6 Dec 2013

11. Y. Cohin, E. Barthel, N. Brun, C. Goldman, S. Le Roy, and E. Søndergård, "Spontaneous formation of copper-silica nanostructures by ion abrasion," Smart Mater. Struct. (In review).
12. S. L. Roy, E. Barthel, N. Brun, A. Lelarge, and E. Søndergård, "Self-sustained etch masking: A general concept to initiate the formation of nanopatterns during ion erosion," J. Appl. Phys. **106**, 094308 (2009).
13. S. Maier, *Plasmonics: Fundamentals and Applications* (Springer, 2007).
14. K. Willets and R. V. Duyne, "Localized surface plasmon resonance spectroscopy and sensing," Annu. Rev. Phys. Chem. **58**, 267–297 (2007).
15. P. C. Wu, M. Losurdo, T.-H. Kim, S. Choi, G. Bruno, and A. S. Brown, "In situ spectroscopic ellipsometry to monitor surface plasmon resonant group-III metals deposited by molecular beam epitaxy," J. Vac. Sci. Technol. B **25**, 1019 (2007).
16. G. F. Walsh, C. Forestiere, and L. Dal Negro, "Plasmon-enhanced depolarization of reflected light from arrays of nanoparticle dimers." Opt. Express **19**, 21081–21090 (2011).
17. N. G. Khlebtsov, A. G. Melnikov, V. a. Bogatyrev, L. a. Dykman, A. V. Alekseeva, L. a. Trachuk, and B. N. Khlebtsov, "Can the light scattering depolarization ratio of small particles be greater than 1/3?" J. Phys. Chem. B **109**, 13578–13584 (2005).
18. T. Oates, M. Ranjan, S. Facsko, and H. Arwin, "Highly anisotropic effective dielectric functions of silver nanoparticle arrays," Opt. Express **19**, 2014–2028 (2011).
19. J. Pérez-Robles, F. Garcia-Rodriguez, J. Yáñez Limón, F. Espinoza-Beltrán, Y. Vorobiev, and J. González-Hernández, "Characterization of sol-gel glasses with different copper concentrations treated under oxidizing and reducing conditions," J. Phys. Chem. Solids **60**, 1729–1736 (1999).
20. S. R. Cloude, "Conditions for the physical realisability of matrix operators in polarimetry," Proc. SPIE **1166**, 177–185 (1989).
21. P. Hauge, R. Muller, and C. Smith, "Conventions and formulas for using the Mueller-Stokes calculus in ellipsometry," Surf. Sci. **96**, 81–107 (1980).
22. J. Gil and E. Bernabeu, "Depolarization and polarization indices of an optical system," J. Mod. Opt. **33**, 185–189 (1986).
23. R. Azzam and N. Bashara, *Ellipsometry and Polarized Light* (North-Holland, 1987).
24. M. Schubert, *Handbook of Ellipsometry* (William Andrew, 2005), chap. Theory and Application of Generalized Ellipsometry.
25. J. M. Sanz, D. Ortiz, R. Alcaraz de la Osa, J. M. Saiz, F. Gonzlez, A. S. Brown, M. Losurdo, H. O. Everitt, and F. Moreno, "Uv plasmonic behavior of various metal nanoparticles in the near- and far-field regimes: Geometry and substrate effects," J. Phys. Chem. C. **117**, 19606–19615 (2013).
26. J. Spanier and I. Herman, "Use of hybrid phenomenological and statistical effective-medium theories of dielectric functions to model the infrared reflectance of porous SiC films," Phys. Rev. B **61**, 10437–10450 (2000).
27. D. E. Aspnes, "Local-field effects and effective-medium theory: A microscopic perspective," Am. J. Phys. **50**, 704 (1982).
28. T. Yamaguchi, S. Yoshida, and A. Kinbara, "Optical effect of the substrate on the anomalous absorption of aggregated silver films," Thin Solid Films **21**, 173–187 (1974).
29. T. Yamaguchi, H. Takahashi, and A. Sudoh, "Optical behavior of a metal island film," J. Opt. Soc. Am. **68**, 1039 (1978).
30. E. D. Palik, *Handbook of Optical Constants of solids* (Academic Press Inc., 1985).
31. H. Kuwata, H. Tamaru, K. Esumi, and K. Miyano, "Resonant light scattering from metal nanoparticles: Practical analysis beyond rayleigh approximation," Appl. Phys. Lett. **83**, 4625–4627 (2003).
32. V. Myroshnychenko, J. Rodriguez-Fernandez, I. Pastoriza-Santos, A. M. Funston, C. Novo, P. Mulvaney, L. M. Liz-Marzan, and F. J. Garcia de Abajo, "Modelling the optical response of gold nanoparticles," Chem. Soc. Rev. **37**, 1792–1805 (2008).

1. Introduction

The spectacular properties of photonic crystals and metamaterials have spurred an increasing interest for the synthesis and characterization of complex biological and manmade nanomaterials. In many cases these materials exhibit a complex 3D organization obtained through self-assembly where objects of various composition, form and size are localized in more or less organized patterns. A systematic approach to the characterization of such materials is often a major hurdle and it hampers the progress in the synthesis. Spectroscopic ellipsometry (SE) and Generalized Ellipsometry (GE) measures the change in polarization state of light upon reflection from a surface over a wavelength range [1, 2]. SE and GE are particularly useful for investigating the pattern formation in self assembly nanostructuring processes [3–5], while for a complete measurement of anisotropic and depolarizing samples, a full Mueller matrix ellip-

#197582 - $15.00 USD Received 12 Sep 2013; revised 18 Nov 2013; accepted 27 Nov 2013; published 6 Dec 2013

sometry (MME) measurement is generally required. Although SE is an established technique for in line production control and real time study of thin film processes, GE and MME have recently been demonstrated as promising techniques for in-situ real time studies of nanostructuring processes [5,6]. For example, spectroscopic MME in the visible range has been successfully utilized to investigate formation mechanism of GaSb nanopillars in ion beam sputtering of GaSb films [5,7–9]. Furthermore, it has recently been shown that ex-situ UV-VIS-NIR spectroscopic MME over a complete azimuthal rotation of the sample and multiple incidence angles is highly sensitive to small tilts of nanopillars away from the surface normal [9]. The spectroscopic MME method is thus a powerful tool to characterize self assembly nanomaterials, and we here aim at extending the use of MME as an additional tool to nano-structured sol-gel materials with plasmonic nanoparticles. Indeed, such a non-destructive characterisation method, can have major advantages compared to the more commonly used direct imaging methods such as Atomic Force Microscopy (AFM), Scanning Electron Microscopy (SEM) and Transmission Electron Microscopy (TEM).

The abundance and interesting optoelectronic properties of CuO has made it an appealing choice for photovoltaic applications [10]. Self assembly of mixed oxide sol-gel film of CuO can introduce new possibilities in photonics and plasmonics. Low energy ion sputtering of CuO sol-gel film is a simple and low cost technique for fabricating a large area of dense nanopillars [11]. Variations of film temperature and ion energies result in the formation of different patterns. The nanopillar formation mechanism can partially be explained by the theory of self-sustained etching mask [12]. According to the latter theory, the metallic Cu on top of the pillars plays the role of an etching mask [11]. Indeed, real time spectroscopic ellipsometry can provide more evidences for the evolution and growth mechanism of nanopillars [5, 7, 8, 12]. Since the presence of metallic copper nanoparticles in the oxide nanopillars supports plasmonic resonances, a strong sensitivity of spectroscopic MME to these resonances can be exploited to reveal more information both about the formation mechanism, and the characteristics of the resonances.

Strong field enhancement and confinement in metallic nanoparticles at localized surface plasmon resonances (LSPR) has inspired many applications in nanophotonics [13]. The spectral position of these resonances can be measured with various spectroscopic methods [14]. The common far field method is to measure either scattering, absorption or extinction cross section over the desired spectral range. The position of LSPRs are highly sensitive to the size and shape of metal nanoparticles as well as optical properties of the host medium. Therefore, any non-uniformity in the sample, leads to broadening of the resonance over the spectral range. Thus the characterization of LSPRs in highly nonuniform self assembled samples become problematic with common methods. LSPRs are resonances in polarizability of a scattering medium, and consequently the polarization of the light scattered from this medium contains information about these plasmon resonances. As a result, ellipsometry is an appropriate tool to study the evolution of such plasmon resonances [15].

Recently, it has been demonstrated analytically and experimentally that a maximum depolarization occurs in the spectral regions of LSPRs [16], and that for anisotropic randomly oriented nanoparticles, the crossed polarized scattering events increase near the plasmon resonance region [17]. However, spectroscopic MME is the most appropriate method to fully measure the polarization properties of a complex scattering medium that show strong anisotropies [18] and is partially depolarizing. Indeed, we expect that the LSPRs will exhibit sharp resonances in both the on and off-block-diagonal Mueller matrix elements, and consequently also in the generalized ellipsometric parameters derived from the so-called Mueller-Jones matrix. Thus we expect that MME is sensitive to both the polarization, here referring to the tensor properties, and the spectral position of the plasmon resonances.

In this paper we use spectroscopic MME with azimuthal rotation of the sample to charac-

#197582 - $15.00 USD Received 12 Sep 2013; revised 18 Nov 2013; accepted 27 Nov 2013; published 6 Dec 2013

terize the nanopillars fabricated by low ion-energy sputtering of CuO sol-gel film [11]. The fabrication and characterization methods are briefly reviewed in section 2, while the measured spectroscopic Mueller matrix elements are presented in Section 3. The spectral behavior of the Mueller matrix elements near the plasmon resonance regions are further investigated in Section 3. The GE parameters are utilized to further reveal the polarization characteristic of each plasmon resonance. Finally, the measured position of two sets of s-polarized and p-polarized plasmon resonances are discussed in terms of the shape of the Cu particles inside the mixed oxide-void matrix.

2. Fabrication and characterization methods

The oxide nanopillars were fabricated by low ion-energy sputtering of a sol-gel film of mixed copper oxide and silica [11] with an initial thickness of typically 400 nm, with further details of the sol-gel procedure in e.g. [19]. The nanopillar growth is initiated when the film is heated and exposed to low energy Ar^+ ions. The pillars tend to point in the direction of the incident ion beam, similar to the formation of GaSb nanopillars reported in previous work [5, 7, 8]. In practice, the ion incidence will slightly deviate from the normal incidence (unless carefully aligned with e.g. optical methods). As a result, the fabricated nanopillars become slightly inclined and consequently the samples have small in-plane anisotropies [9]. Optical studies of two different samples with the fabrication parameters given in Table 1 are reported here.

Table 1. Fabrication parameters for the samples.

Sample	Temperature °C	Flux mA cm^{-2}	Exposure time s	Ion energy keV	Pillar density μm^{-2}
A	300	0.2	360	1	10.7
B	400	0.6	120	1	3.2

Figure 1 shows representative SEM images of the two samples. It is observed that the distribution of the pillars is spatially non-uniform. A further analysis of the corresponding AFM images [11], shows that the heights of the pillars in sample A are distributed around approximately 180 nm, see Fig. 2. For sample B, the distribution of the pillar height is large and asymmetric towards higher pillar heights, see Fig. 2. Indeed, for sample B, pillars nearly 700 nm long are observed, and there appears to be several distinct distributions around approximately 180, 300 and 400 nm.

Cu particles were directly observed on top of, inside and on the side of the nanopillars, using scanning transmission electron microscope images [11], and they were reported to form as a combined result of the sputtering process and the substrate temperature during sputtering. Cohin et al. [11] further reported that single-crystal Cu particle segregate to the top of the pillars, whereas the pillars were determined to be mainly of silica. However, the pillars also appeared to have a partially nanocrystalline Cu core, as schematized in Figs. 3(a-c) [11]. The top Cu particles were shown to be single Cu crystals [11], and most likely contribute as sputtering masks in the abrasion process during the growth of the pillars. In some cases, thin Cu wires were observed on one side of very long pillars, as schematized in Fig. 3(e) [11]. As a result, it is expected that any observations of plasmon resonances will be broadened in the far field.

The spectroscopic MME measurements were performed using an RC2 spectroscopic Mueller matrix ellipsometer from *J.A. Woollam Company*. The instrument is a complete Mueller matrix system based on two rotating retarders. The illumination part consists of a 150 W Xe lamp with a source pin-hole of 100 μm and collimation optics giving an initial beam waist diameter of approximately 3 mm. The detection system consists of a combination of an InGaAs and a Si spectrograph, where the data are recorded at wavelengths from 210 to 1700 nm (0.73 to 5.9

#197582 - $15.00 USD Received 12 Sep 2013; revised 18 Nov 2013; accepted 27 Nov 2013; published 6 Dec 2013

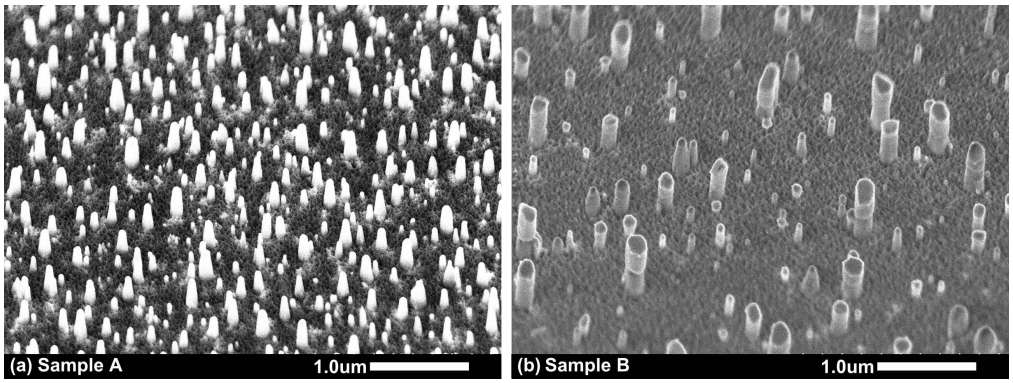

Fig. 1. SEM images of the surface of samples A and B. The view angle is 40° in both images.

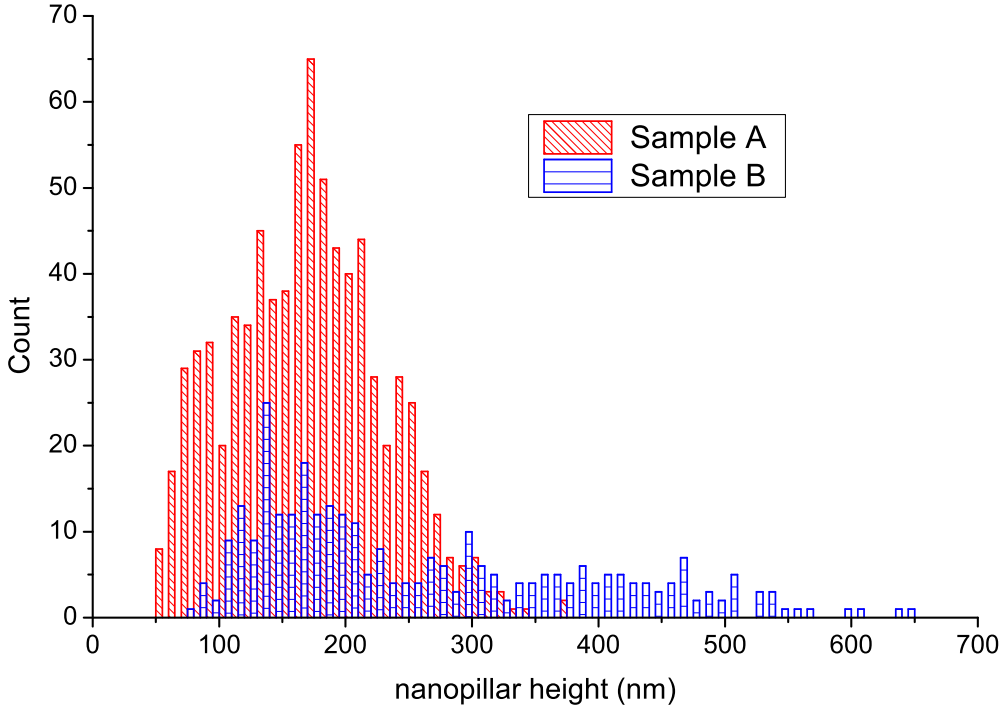

Fig. 2. Height distribution for sample A and B estimated from the AFM images (not shown).

#197582 - $15.00 USD Received 12 Sep 2013; revised 18 Nov 2013; accepted 27 Nov 2013; published 6 Dec 2013

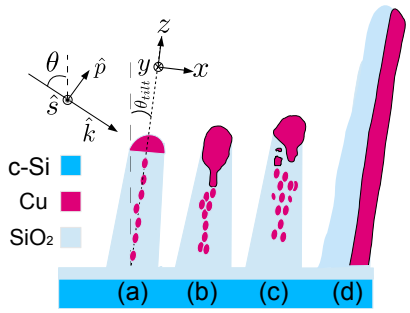

Fig. 3. Sketch of the nanopillars with Cu nanoparticles on top, inside or on the side of the nanopillars [11]. Pillar (a) and (d) represent the phenomenological model, while (b) and (c) shows variations in the Cu-cap as reported in Cohin et al. [11]. The figure also shows the local geometry of the tilted nanopillars with the z axis parallel to the pillars tilted a small angle θ_{tilt} away from the sample normal, and the x and y axis perpendicular to the pillars. x, y and z are proposed to form the principal axis of the diagonal dielectric tensor for the oxide nanopillars/Cu particles system. The components of the incident field, similar to Fig. 4 is also drawn, where θ is the incidence angle with respect to the substrate surface normal.

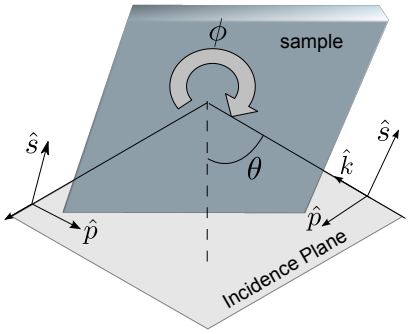

Fig. 4. Sketch of the measurement system configuration, showing the incidence plane, the incidence angle (θ) and the azimuthal rotation of the sample (ϕ).

eV) with a resolution of 2 nm for wavelengths $>$ 1000 nm, and 1 nm for wavelengths $<$ 1000 nm. For sample A, the measurements were performed using multiple angles of incidence (θ) from 50° to 70° with a complete 360° azimuthal rotation of the sample (ϕ) around the surface normal, see Fig. 4, both in steps of 5°. The sample was carefully realigned at each incidence angle in order for the optical spot to be immobile upon rotation of the sample. For Sample B, the complete azimuthal rotation of the sample was performed at 70°, while multiple angles of incidence (θ) from 50° to 70°in steps of 5°was performed with an azimuthal orientation of 45 degrees. These two samples were selected from similar Mueller matrix measurements of a sample series of ten samples fabricated on c-Si, with similar features. Micro focusing probes of 80 mm focal length was used to limit the spot size to approximately 150 µm (spot-size measured at normal incidence), consequently reducing the influence of spatial inhomogeneities. The physical realizability of the measured Mueller matrices are evaluated by calculating a quantitative measure of the system fidelity, as introduced in [20]. Even with the focussing probes, the system fidelity noise was in general low (less than -30 dB), while in the worst cases it was less than -16dB.

#197582 - $15.00 USD Received 12 Sep 2013; revised 18 Nov 2013; accepted 27 Nov 2013; published 6 Dec 2013

3. Results and analysis

Figure 5 shows the measured spectroscopic 4×4 Mueller matrix as a polar color map where the photon energy in the range 0.73 - 5.9 eV is mapped to the radial direction, and the azimuthal angle (ϕ) is mapped to the polar angle. All the data are presented such that ϕ=0° corresponds to a sample rotation resulting in a maximum observed anisotropy (which we later in the paper propose to be the azimuthal orientation angle of the sample corresponding to the pillars tilted in a plane perpendicular to the incidence plane). Figure 5 is a complete presentation of the spectroscopic data with a 360° azimuthal rotation of samples A and B, for a given angle of incidence. The Mueller matrices of samples A and B are plotted for the incidence angles of 65° and 70°, respectively. Note that all m_{ij} elements have been normalized to the total intensity M_{11}.

It is observed that for both samples in Fig. 5, the block-diagonal elements have higher amplitudes compared to the off-block-diagonal elements, and they contain spectral features that can be mistaken as interference fringes. There are also small variations in the block diagonal elements upon azimuthal rotation, but these variations are masked by the much larger amplitudes of the spectrally dependent features. On the other hand, the off-block-diagonal elements, which are nominally zero for isotropic materials and uniaxial materials with the extra-ordinary axis perpendicular to the sample surface, show features that appear anti-symmetric by 180° upon rotation of the incidence plane. Two sets of rings are observed in the off-block-diagonal elements, with an inner ring typically located in the range 1 to 3 eV and an outer ring typically located in the range 3 to 5 eV.

The Mueller Jones matrix for a non-depolarizing anisotropic sample [21] shows that these rings are the result of polarization coupling between s- and p-polarized light. Furthermore, the observed 180° asymmetry is similar to the uniaxial anisotropy observed for tilted and slightly tilted GaSb nanopillars in previous work [8, 9]. In the latter case, the in plane projection of the direction of the tilt-axis resulted in an in-plane anisotropy. However, a small tilt of the low density SiO_2 pillars should not result in an anisotropy causing such large amplitudes in the off-diagonal elements as observed in Fig. 5. It is therefore proposed that these rings are localized plasmon resonances resulting from Cu nanoparticles within or on top of the oxide pillars. Indeed, such Cu particles were directly observed in scanning transmission electron microscope images reported by Cohin et. al. [11], as briefly described in Section 2, and this a-priori information is visualized in the schematic diagram in Fig. 3 [11].

Having studied the symmetry of the spectroscopic Mueller matrix upon azimuthal rotation, we now focus on the spectroscopic features. We select to study the spectroscopic data for azimuthal rotations of the samples with steps of 45°, as these angles will capture most of the symmetric features observed in Fig. 5. Figure 6 shows the upper right triangular elements of the Mueller matrix as a function of photon energy for samples A and B. The depolarization index [22] calculated from the Mueller matrix is shown in the bottom figure, while the total intensity is shown in the top figure. We observe that there is a distinct correlation between the structures in the off-block-diagonal elements $(m_{13}, m_{23}, m_{14}, m_{24})$ and the block-diagonal elements (m_{12}, m_{33}, m_{34}). There is also a certain correlation with the depolarization index and the total intensity. The positions indicated by the red lines show the maxima of the m_{33} element.

A careful comparison of the structures in the Mueller matrix elements in Fig. 6, shows that the peaks in the m_{33} element correlate to the zero crossing in the m_{14} element, and simultaneously a maximum of the m_{24} element. The m_{34} element shows certain corresponding extrema. On the other hand, the m_{12} element shows a maximum and a minimum around the peaks of the m_{33} element. Furthermore, the extrema of the m_{12} element correlate to the peaks of the m_{14} element. Finally, the dip in the intensity occurs at the positions of the peaks in the depolarization. It should be noted that the m_{33} element of sample B have two broad maxima between photon

#197582 - $15.00 USD Received 12 Sep 2013; revised 18 Nov 2013; accepted 27 Nov 2013; published 6 Dec 2013

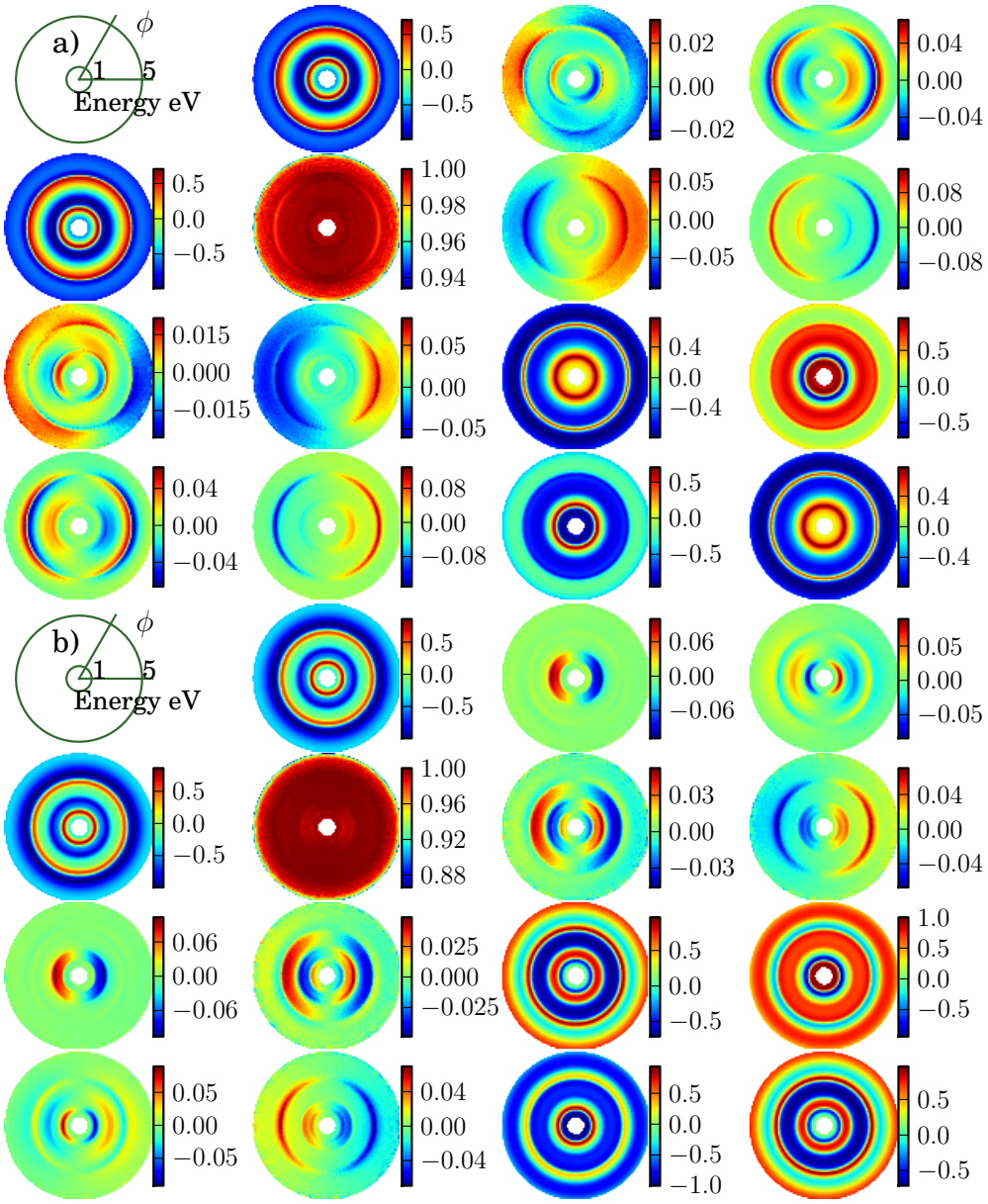

Fig. 5. Measured spectroscopic Mueller matrix for a complete 360° azimuthal rotation of the samples a) A and b) B with incidence angles of 65° and 70°, respectively. The radial and azimuthal axes correspond to photon energy and in plane rotation, respectively.

#197582 - $15.00 USD Received 12 Sep 2013; revised 18 Nov 2013; accepted 27 Nov 2013; published 6 Dec 2013

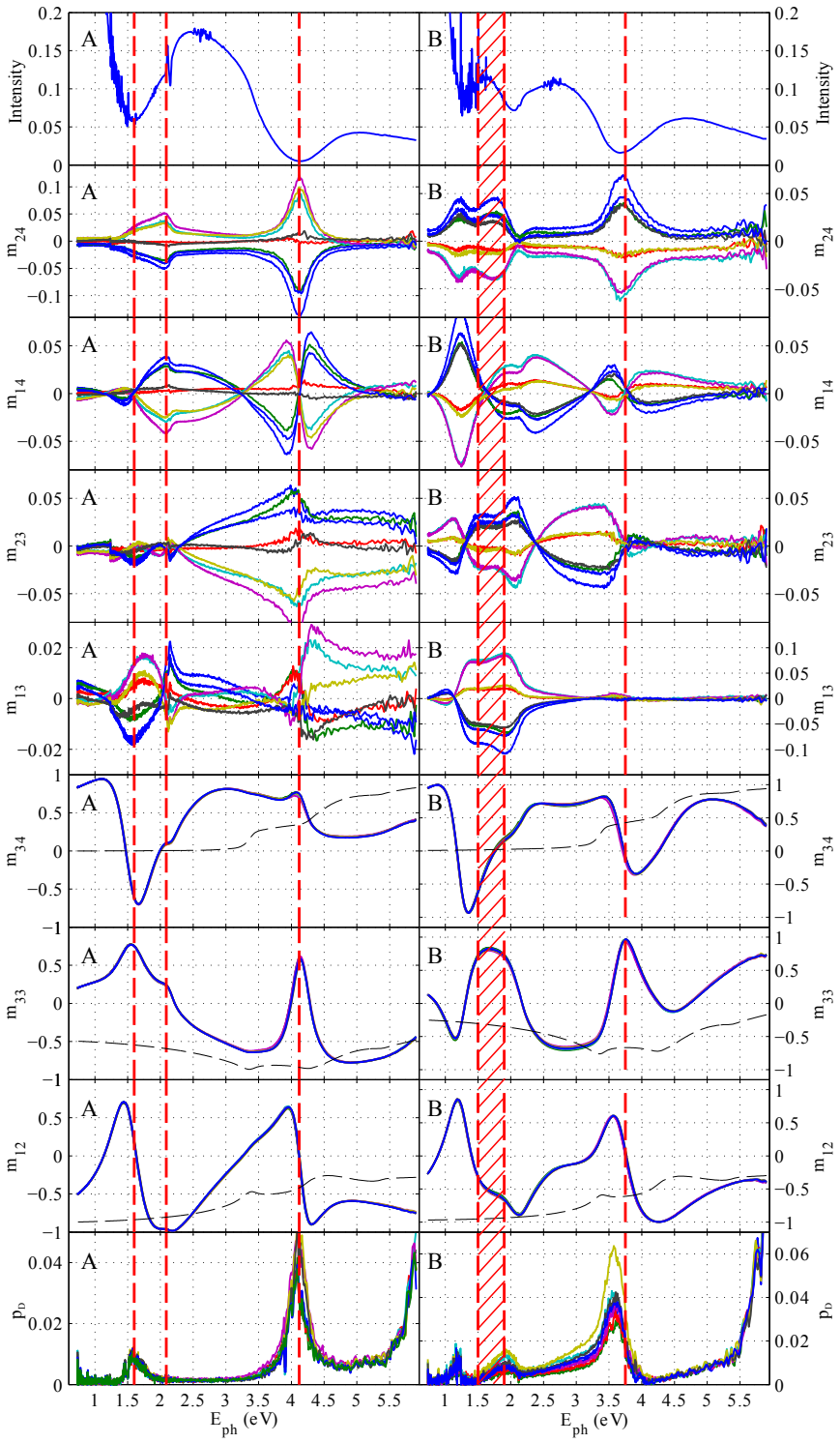

Fig. 6. Total (not normalized) reflected intensity (top figure), the depolarisation index (bottom figure) and selected Mueller matrix elements for a complete azimuthal rotation of samples A and B versus photon energy with incidence angles of 65° for sample A and 70° for sample B. The positions indicated by the red lines show the maxima of m_{33} element and dashed black lines are calculated Mueller matrix elements from the air/c-Si interface.

#197582 - $15.00 USD Received 12 Sep 2013; revised 18 Nov 2013; accepted 27 Nov 2013; published 6 Dec 2013

energies of 1.5 eV and 1.9 eV that are not resolved, and form a wide maximum in this region. However, the Mueller matrix elements follow a similar trend to the above, at the photon energy in the center of this region, as shown by the shaded red region in Fig. 6.

These observations allow us to infer that the rings in the block-diagonal elements in Fig. 5 are also strongly related to the localized plasmons, and are not interference fringes. Sample A has the highest density of pillars (pillar density estimated to 10.7 μm^{-2}), but a rough estimate of the average pillar distances is of the order of 300 nm, i.e. quite large with respect to the probing wavelengths. There is thus an overall low density of pillars in addition to the distribution of the pillar heights, as seen from Figs. 1 and 2. As a result, the metal-oxide nanopillars studied here should not be regarded as a film on a substrate, but rather as free standing scattering particles on top of, within or on the side of oxide-pillars on a substrate. Consequently, the system is proposed to be more appropriately modelled as a combination of a scattering problem and a standard dichroic retarder for the bottom film-substrate reflection. The fully developed nanopillars can possibly be modelled by forming the scattering Mueller matrices for the localized plasmons $\mathbf{M}_{LP}^{\text{in}}$ and $\mathbf{M}_{LP}^{\text{out}}$, in addition to the film-substrate reflection Mueller matrix $\mathbf{M}(\psi,\Delta)$, where one further assumes that for the particles, it is mainly the forward scattered light that is detected.

$$\mathbf{M} = \mathbf{M}_{LP}^{\text{out}}\mathbf{M}(\psi,\Delta)\mathbf{M}_{LP}^{\text{in}} \tag{1}$$

It is clear that an even more complicated situation will take place during the initial phase of the sputtering process, where the sol-gel film will remain underneath the pillars, although the corresponding interference fringes from the thick CuO oxide sol-gel film on the c-Si substrate can be correctly represented by the matrix $\mathbf{M}(\psi,\Delta)$. On the other hand, it is envisaged that real time spectroscopic MME would supply additional information in order to further reveal the appropriate optical model for the optical response of this complex system.

The plasmon resonances are not as easily detected for all samples, as is demonstrated by sample B. Sample B has a lower density of pillars ($\approx 1\ \mu m^{-2}$) and a larger distribution of pillar heights compared to sample A, see Fig. 2, but it can still be favourably studied with MME, as shown in Fig. 6. The correlation between the m_{24} and m_{14} elements is less obvious for sample B, and similarly m_{33} only shows a single broad low energy peak. Furthermore, the depolarization appears to take place somewhat below the apparent dip in the intensity, particularly for the resonance around 2.2 eV.

Figure 7 shows the dependency of the Mueller matrix elements on the angle of incidence, similarly to Fig. 6, for the azimuthal orientation of 0° for sample A, and 45° for sample B. Figure 7 also shows the total intensity (top figure) and the depolarization index [22] (bottom figure). It is observed that the shifts in the resonances are small for the low energy resonances. This means that the colour appearance of the sample is similar, independent of viewing angle. This phenomenon was also observed on similar samples manufactured on glass, where a yellow colour was observed by the eye at all viewing angles. The latter observation supports our interpretation that the observed resonances are mainly of plasmonic origin, and not a result of interference (interference causes a colour shift upon changing the viewing angle/incidence angle). However, some shifts in the resonance positions are observed, which is particularly striking at the high energy resonances in the range 3.5-4.5 eV. Note that the total intensity (not normalized) is not an absolute value (i.e. each spectrum is scaled by unknown constant), as an automatic attenuator filter in the illumination beam could not be controlled at the various incidence angles.

With a complete Mueller matrix ellipsometer one may choose between analyzing the complete Mueller matrix, or by neglecting the depolarization, find the closest corresponding Jones matrix and study the generalized ellipsometric parameters [23, 24]. This method can be used as long as the depolarization is small. The ellipsometric parameters are defined as the ratio of

#197582 - $15.00 USD Received 12 Sep 2013; revised 18 Nov 2013; accepted 27 Nov 2013; published 6 Dec 2013

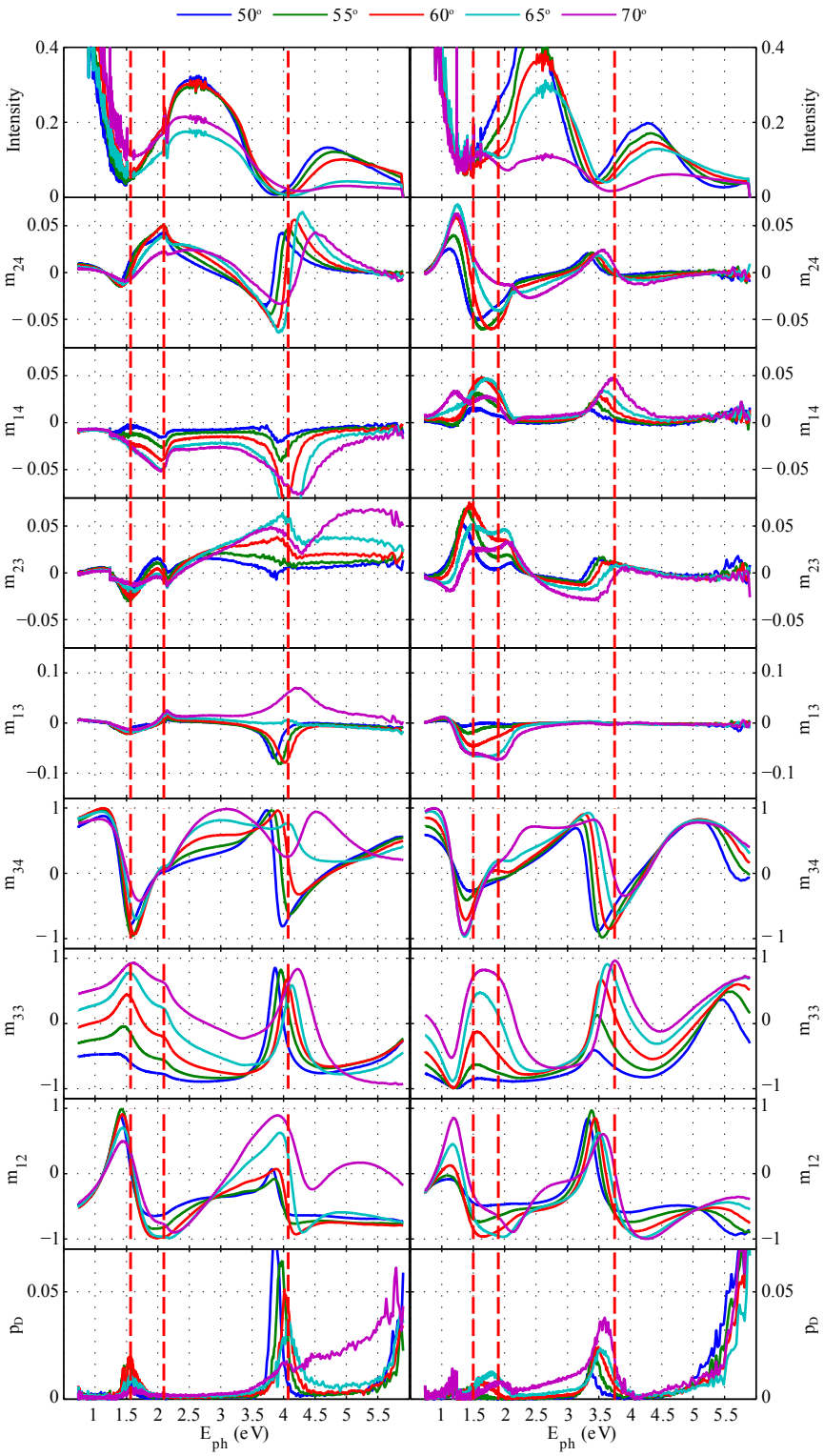

Fig. 7. Total intensity (top figure), selected Mueller matrix elements and depolarization index (bottom figure) for samples A and B versus photon energy with different incidence angles and azimuthal angles of 0° for sample A and 45° for sample B.

#197582 - $15.00 USD Received 12 Sep 2013; revised 18 Nov 2013; accepted 27 Nov 2013; published 6 Dec 2013

the reflection coefficients of orthogonal polarization states. In isotropic materials there are no coupling between orthogonal polarization states and therefore the Fresnel coefficients r_{sp} and r_{ps} are zero, corresponding to zero off-block-diagonal elements of the Mueller matrix. Here r_{ps} denotes conversion from p-polarized to s-polarized light, while r_{sp} denotes conversion from s-polarized to p-polarized light. In this case the generalized ellipsometric parameters, i.e. the relative amplitudes ψ, ψ_{ps},ψ_{sp} and the phase shifts Δ, are defined by:

$$\frac{r_{pp}}{r_{ss}} = \tan\psi\, e^{\mathrm{i}\Delta}, \quad \frac{r_{sp}}{r_{ss}} = \tan\psi_{sp}\, e^{\mathrm{i}\Delta_{sp}}, \quad \frac{r_{ps}}{r_{pp}} = \tan\psi_{ps}\, e^{\mathrm{i}\Delta_{ps}}. \tag{2}$$

Figure 8 shows the generalized ellipsometric parameters of samples A and B with an azimuthal angle of 0°(i.e. at maximum observed anisotropy), where the parameter ψ basically conveys the same information as m_{12}. However, ψ_{sp} and ψ_{ps} appears to take more appropriate peak shapes that can facilitate the localization of the plasmon resonances. The non-uniformity of both the supporting nanopillars, the variety of Cu-particle sizes, shapes and locations within or on top of the nanopillars, are probable causes for the broadening of the plasmon resonances.

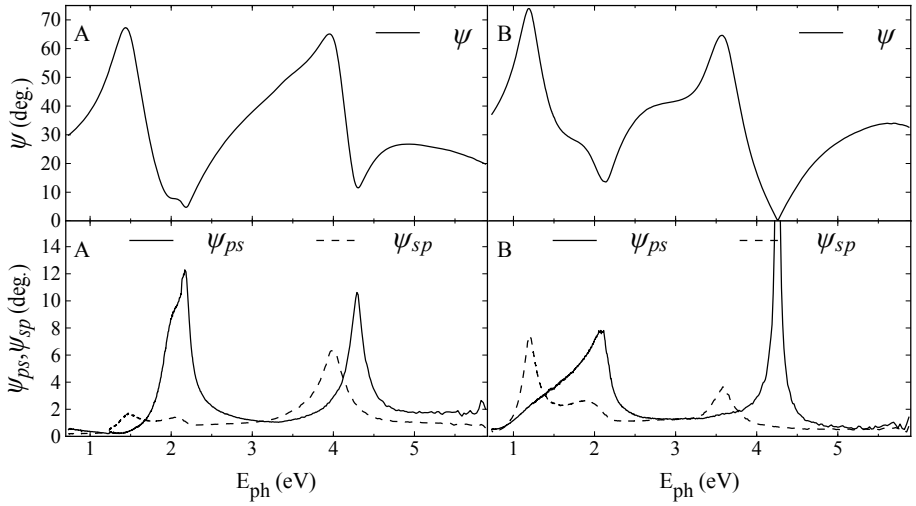

Fig. 8. Generalized ellipsometric parameters ψ, ψ_{sp} and ψ_{ps} of samples A and B for the azimuthal angle 0°. The parameters are calculated from the Mueller matrix in Fig. 6.

The above data are proposed interpreted phenomenologically as follows. The peaks in ψ, or m_{12}, are related to dichroism as a result of the localized plasmon resonances, with the principal "absorption"-axis in the s-polarized component (i.e. perpendicular to the incident plane). In the local geometry shown in Fig. 3, the Cu particles are pictured as suspended by the oxide nanopillars, resulting in a uniaxial system with dielectric functions ε_{e} along z i.e. parallel to the pillars, and ε_o perpendicular to the pillars. Then a resonance with an observed s-character is the result of mainly a resonance in ε_o. The maximum in m_{12} and the dip in the intensity (for the low energy resonances) may be understood as the combination of a Brewster effect from the silicon substrate (working nearly as an s-polarizer near the pseudo-Brewster angle) accompanied by an absorption of s-polarized light through the plasmon resonance in the ε_{o} component. As the incident polarization state becomes mainly p-polarized through the plasmon resonance, the subsequent reflection near the Brewster angle at the substrate interface result in the strong dip in the intensity, see top Figs. 6 and 7. Figure 6 also shows that m_{12} (dashed black lines) calculated for an air/c-Si interface is large and negative, while at the resonance it peaks towards

#197582 - $15.00 USD Received 12 Sep 2013; revised 18 Nov 2013; accepted 27 Nov 2013; published 6 Dec 2013

+1, interpreted as a nearly complete absorption of s-polarized incident light. This resonance causes further a strong retardance effect, which results in a peak in ψ_{sp} which correlates to a peak in the m_{33} element.

The dips in ψ, or m_{12}, are believed to be related to a dichroism due to the localized plasmon resonance with the principal axis in ε_e, which strongly contributes to the absorption of the p-polarized component of the incident field. As mainly s-polarized light is reflected from the substrate near the pseudo-Brewster angle, the latter resonance only results in a minor dip in the total intensity, but gives a peak in ψ_{ps}, which also correlates to a peak in the m_{33} element.

Although the variations in the resonance positions as a function of angle of incidence needs further work, one may argue that at lower angles of incidence, the p- and the s-components of the incoming field has both an x (or an ordinary component in the x, y-plane), and a z (extraordinary) component. At higher incidence angles, the p-component of the field picks up more of the z component, and hence one expects to observe a shift of the spectral location of the observed resonance of p-polarisation character from a mixed resonance in ε_o and ε_e towards a single resonance in ε_e. This hypothesis fits reasonably well to the observations from sample A, while sample B appears to need a more complex interpretation.

Given the above phenomenological interpretation, a combined analysis of the above data, allow us to make an approximate determination of the spectral position of the modes as well as its polarization characteristics. The resonances are divided into four main resonances LP1-LP4 and their position and polarization characteristics are given in Table 2.

Table 2. Rough estimate of position of the localized plasmon resonances and their polarization characteristics for samples A and B

Sample	LP1 (eV)	LP2 (eV)	LP3 (eV)	LP4 (eV)
A	1.6 (s-pol)	2.1 (p-pol)	3.9 (s-pol)	4.3 (p-pol)
B	1-1.3 (s-pol)	1.5-2.3 (p-pol)	3.4-3.7 (s-pol)	4-4.3 (p-pol)

Two pairs of resonances are found for both samples. For sample A, the resonances are split in a low energy resonance at 1.6 eV of principally s-character and a high energy resonance at 4.3 eV of principally p-character, a low energy resonance at 2.1 eV of p-character and a high energy resonance at 3.9 eV of s-character. Sample B does on the other hand show a large distribution of resonances, which correlates well with the analysis of the AFM and SEM images. The most disputed resonances, are those here allocated in the range 3.5-4.3 eV, often neglected due to the large imaginary part of the dielectric function of bulk Cu, as a result of interband transitions. The occurrence of such resonances for various metals in the UV region was recently discussed by Sanz et al. [25], where a UV resonance at non-normal incidence for Cu particles was neither rejected nor confirmed. A recent example of UV localized plasmon resonances was reported for hemispherical Ga nanoparticles on sapphire, detected using spectroscopic ellipsometry [15]. The single peak in the Mueller matrix elements m_{33} and m_{24}, and the dip in the total intensity, for the UV resonances in Figs. 6 and 7, shows that there is a reasonable doubt that the LP3 and LP4 are separate resonances, although the generalized ellipsometric parameters in Fig. 8 indicate such a double resonance.

We infer that the observed depolarization is due to a physical effect taking place at the resonance, and not a system calibration artifact due to e.g. low light intensity, based on the following arguments. It is expected that an incomplete coverage or inhomogeneous spatial distribution of the pillars and the Cu particles results in depolarization. Furthermore, small Cu particles are strongly radiating at the resonance, and some of this radiation is collected by the micro-focus lens used in the system. Depending on the radiation pattern and hence the type of scatterer, the

#197582 - $15.00 USD Received 12 Sep 2013; revised 18 Nov 2013; accepted 27 Nov 2013; published 6 Dec 2013

detected light may become depolarized. This is in principle similar to including a small contribution of reflected light from the particles, which add incoherently to the forward scattered light, subsequently reflected by the substrate. However, we were not able to detect non-specular radiation with a commercial scatterometer using monochromatized white light illumination.

An accurate interpretation of the data involves scattering calculations of small anisotropic shaped metal particles that have an orientation which resembles the nanopillar orientation. However, since the particles may be on top of the pillars, inside the pillars or on the side of the pillars as shown in Fig. 3, a rigorous determination of the resonances for such a disordered system is challenging. On the other hand, effective medium theory (EMT) can sometimes be used to explain the localization and splitting of the resonances as well as the measured anisotropy, although the dimensions of the pillars are generally outside the validity of EMT. For a phenomenological model, it still appears useful to consider the particle scattering matrix in terms of EMT [26–29], similar to e.g. liquid crystals. Note that the variation of the EMT proposed by Yamaguchi et al. [28,29], takes the substrate effect (here c-Si) into account. However, in the current case, the substrate effect is negligible as the Cu particles are suspended in the nanopillars up to several hundred nanometers away from the substrate.

Figure 9 shows the spectral position of the plasmon resonances of Cu nano-particles inside nano-pillar matrix calculated using generalized EMT [5, 26]. The calculation is carried out using bulk dielectric function of Cu and SiO_2 reported in [30]. The dependence on the volume fraction (fill-factor) of the nanopillars by neglecting retardation effect is plotted in Fig. 9(a). First we consider spherical Cu particles within the anisotropic host medium of an oxide pillar in air. We represent the host medium by an uniaxial effective medium consisting of SiO_2 nanopillars and void, where the fill-factor of the nanopillars, $f_{nanopillar}$=1-f_{void}, where f_{void} is the volume fraction of the void. The host medium becomes anisotropic if the oxide pillars are regarded as cylinders with depolarization factors L_z=0 and $L_{x,y}$=0.5. We propose to tentatively estimate the Froehlich condition for a spherical Cu-particle inside the uniaxial host material, by using the components of the effective medium for the ordinary and extra-ordinary component of the host material. Using this approximation, the red solid and dashed lines in Fig. 9 correspond to the position of LSPR's perpendicular and parallel to the nanopillars, respectively. In principle, even for a spherical Cu-particle, this approach leads to two orthogonal resonance modes that are slightly split, but both located around 3.4 eV. However, the uniaxial host material using this approach, cannot explain the observed low and high energy resonances. Note that a host medium of Cu_2O, SiO_2 and air would result in a wider range of resonances and a larger splitting.

Now, we consider the case where the Cu particles take a prolate shape. We further assume that the Cu particles have the same principal axis as the surrounding oxide nano-pillar. The L_z and L_x in the legend of Fig. 9 represent the depolarization factors of the Cu particles parallel and perpendicular to the pillars, respectively. The position of the s-polarized localized plasmon resonances, defined by an absorption line (resonance) perpendicular to the incidence plane, are shown by solid lines. The positions of the localized plasmon resonances along the pillars, which result in the main contributions to the absorption of p-polarized light, are shown by the dashed lines. The s-polarized resonances are only allowed for lower energies for a disk-shaped Cu particle ($L_z > L_x$, $L_x \simeq L_y$). In this case, the p-polarized resonances will be shifted to higher energies. As a result, the observed low energy s-polarized resonance accompanied with a high energy p-polarized resonance must be dedicated to disk shaped particles. On the other hand, needle shaped Cu particles ($L_z < L_x$, $L_x \simeq L_y$) parallel to the oxide pillars have p-polarized resonances located at lower energies, accompanied with an s-polarized resonance at higher energies.

In Fig. 9(b), the retardation effect is taken into account by using the empirical formula re-

#197582 - $15.00 USD Received 12 Sep 2013; revised 18 Nov 2013; accepted 27 Nov 2013; published 6 Dec 2013

ported in [31], using a constant fill-factor of 0.1. The retardation effects become significant when the size of the particles increases and causes a red shift of the resonances. When the size of particles become comparable to the resonant wavelength (approximately one third of the resonant wavelength), the quadropole modes start to appear. The position of quadropolar resonances blue shift with respect to the position of dipolar resonances [32]. In our case the particle sizes does in general not exceed 100 nm. Although at this size the retardation effects start to play an important role, the quadropole resonances can not be excited. The long antennas on the side of certain pillars is an exception.

On the other hand, the nanopillars are too far away from each other in such a low density sample, for the interaction between Cu particles in neighboring pillars to excite multipolar plasmon resonances. Several small particles (or e.g. dimers) in close proximity inside a pillar could be imagined to result in a longitudinal and transverse mode splitting of the plasmon resonances [13], but this hypothesis was rejected in such a disordered sample, as it is unlikely that all pillars have identical geometries. However, the latter effects can in principle contribute to the broadening of the plasmon resonances.

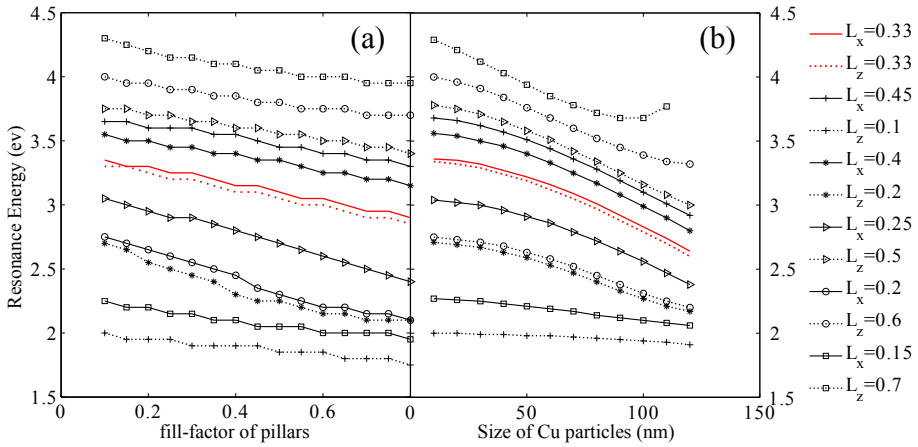

Fig. 9. a) The spectral position of the plasmon resonances of Cu nano-particles estimated using the Froehlich condition, with the host material (nano-pillar/void matrix) calculated using the generalized EMT for an uniaxial material, as a function of the volume fraction (fill-factor) of the oxide nanopillars. The depolarization factors for the oxide nanopillars (SiO_2) in the host matrix was L_z=0 and $L_{x,y}$=0.5. b) The estimated spectral position of the resonances as a function of the Cu particle size, using a fill-factor of the oxide pillars of 0.1, in the EMT for the host matrix. In both figures, the legends represent the depolarization factors used to model the shape of the Cu-particle inclusions in the host matrix.

The pair of resonances interpreted to be at 1.6 eV (s-pol) and 4.1-4.3 eV (p-pol) for sample A are thus in terms of EMT a result of disk shaped Cu particles, while the resonance at 2.1 eV (p-pol) accompanied with resonances around 3.9 eV (s-pol) are a result of a more needle shaped Cu particles.

A similar trend can be observed for sample B, although the resonances are here smeared out due to a larger distribution of the pillar heights. Such disk shaped Cu particles can be found on top of the pillars, i.e. acting as the self-sustained etching mask during the nanopillars growth, while the needle shape particles could be from either the inside of the oxide nanopillars (corresponding to the majority of the particles), or such as the needle shaped particles found on the side of some of the long nanopillars as schematically shown in Fig. 3.

#197582 - $15.00 USD Received 12 Sep 2013; revised 18 Nov 2013; accepted 27 Nov 2013; published 6 Dec 2013

4. Conclusion

We have shown that spectroscopic Mueller matrix ellipsometry is an appropriate far field method to investigate the broadened plasmon resonances of non-uniform self assembled samples, such as the mixed oxide nanopillars fabricated by low energy ion sputtering of sol-gel mixed oxide films containing Cu-oxide nanoparticles. Dips in the total intensity, peaks in the depolarization, peaks in m_{33}, and minima and maxima of m_{12} are observed to be correlated at the spectral position of the localized plasmon resonances resulting from Cu particles on top of, inside or on the side of the nanopillars that mainly consist of silica. Since the slight tilt of oxide pillars without Cu particles can only result in minor deviations of the off-block-diagonal elements from zero, the strong signal in these elements at the plasmon resonances is a result of the Cu nanoparticles, which further supports the interpretation of the features in the block-diagonal elements. The generalized ellipsometric parameters ψ_{ps} and ψ_{sp} exhibit clear peaks at plasmon resonance regions as a result of the slight anisotropy in the samples. These parameters present two sets of the s-polarized and p-polarized plasmon resonances. An interpretation of the position of these resonances using effective medium theory, indicates the presence of both disk shaped and needle shaped Cu particles. The in plane anisotropy of the pillars is small due to the low pillar density, but an enhanced anisotropy is observed near the plasmon resonances. Although the out of plane anisotropy of the pillars leads to a small mode splitting of the s-polarized and p-polarized plasmon resonances, it is the shape and orientation of the Cu particles forced by the anisometric shape of the nanopillars that is believed to cause the mode splitting. On the other hand, the polydispersity of the nanopillars has some effect on measured Mueller matrix elements, but is generally small for such a low density of pillars, while the effect of polydispersity appears more pronounced near the plasmon resonances. The plasmon resonances are broadened due to both polydispersity of Cu particle shape and size, as well as the polydispersity of the supporting nanopillars, i.e. the surrounding material for the plasmonic Cu particles. The strong sensitivity to the localized plasmons produced by the Cu particles in the low density nano-pillar host matrix, makes Mueller matrix ellipsometry a suitable technique for studying the related complex polarization phenomena. However, commercial ellipsometric thin film software appears unsuited for the exact modeling, and future work will focus on developing suitable modelling which will allow us to directly fit the lineshapes of the plasmon resonances. As the reported UV-resonances are the most disputed, it is particularly interesting to search further evidence for the latter observations. Finally, real time in-situ investigation using MME during the fabrication process is envisaged to reveal more details of the formation process.

Acknowledgment

This work was supported by “Norwegian Research Center for Solar Cell Technology” (project num. 193829).

#197582 - $15.00 USD Received 12 Sep 2013; revised 18 Nov 2013; accepted 27 Nov 2013; published 6 Dec 2013